EFFECT OF TRANSVERSE RADIATION DEFOCUSING IN POST-SATURATION REGIME OF HIGH-GAIN X-RAY FREE ELECTRON LASER*

C.-Y. Tsai[1][†], J. Wu[‡], C. Yang[1], M. Yoon[2], and G. Zhou[3]
SLAC National Accelerator Laboratory, Menlo Park, California, USA
[1] also at NSRL, University of Science and Technology of China, Hefei, Anhui, China
[2] also at Department of Physics, Pohang University of Science and Technology, Pohang, Korea
[3] also at Institute of High Energy Physics, and UCAS, Chinese Academy of Sciences, Beijing, China

Abstract

When untapered high-gain free electron laser (FEL) reaches saturation, the exponential growth ceases and the radiation power starts to oscillate about an equilibrium. For a high-gain tapered FEL, although the power is enhanced after the first saturation, it is known that there is a so-called second saturation point where the FEL power growth stops. In addition to the sideband instability, lack of transverse radiation focusing in the post-saturation regime can be another major reason leading to occurrence of the second saturation. In this paper we study the transverse diffraction effect and its impact on tapered FEL in the post-saturation regime. The study is carried out analytically together with three-dimensional numerical simulation.

THEORETICAL FORMULATION

We begin by formulating the problem based on the following single-particle Hamiltonian [1]

$$\mathcal{H}(\theta_j, \eta_j; \hat{z}) = \frac{(\eta_j - \eta_R)^2}{2f_R} - i\frac{f_B(\hat{z})}{f_R(\hat{z})}\left(\mathcal{E}e^{i\theta_j} - \mathcal{E}^*e^{-i\theta_j}\right) \quad (1)$$

where $j(=1, 2, 3, \cdots, N_e)$ is the index for each individual particle and N_e is the total number of macroparticles (electrons). $\theta = (k_R + k_u)z - \omega_R t$ is the electron phase with respect to the radiation, $k_u = 2\pi/\lambda_u$ with λ_u the undulator period, $k_R = 2\pi/\lambda_R$, and $\omega_R = ck_R$, $\eta \equiv [\gamma - \gamma_R(0)]/\rho\gamma_R(0)$, with $\gamma_R(0)$ the initial Lorentz relativistic factor, is the normalized energy deviation with respect to the dimensionless FEL or Pierce parameter $\rho = \frac{1}{\gamma_R(0)}\left(\frac{4\pi e^2 n_0 K_0^2}{32 m_0 c^2 k_u^2}\right)^{1/3}$ with e the charge unit, n_0 the volume density of the electron beam, m_0 the electron rest mass and $\eta_R = [\gamma_R - \gamma_R(0)]/\rho\gamma_R(0)$. The longitudinal coordinate is normalized according to $\hat{z} = 2k_u\rho z$. In the case of undulator tapering, the electron reference energy follows $\gamma_R(\hat{z}) = \gamma_R(0)f_R(\hat{z})$ where $f_R(\hat{z}) = \sqrt{\frac{1 + K^2(\hat{z})/2}{1 + K_0^2/2}}$ and $K(\hat{z}) = f_B(\hat{z})K_0$ with K_0 the (peak) dimensionless helical undulator parameter. Here $|\mathcal{E}| = |E|/\sqrt{4\pi n_0 \rho\gamma_R(0)m_0 c^2}$ is the normalized amplitude of the electric field E.

From Hamilton's equations, we can obtain the single-particle equations of motion for the electron phase and energy deviation. The normalized electric field, governed by the 1-D paraxial wave equation, can be expressed as

$$\frac{\partial \mathcal{E}}{\partial \hat{z}} = \frac{f_B(\hat{z})}{f_R(\hat{z})}\left\langle e^{-i\theta}\right\rangle \quad (2)$$

where the bracket $\langle...\rangle$ denotes an ensemble average over the electron beam in the steady state (or a single bunch slice).

It is straightforward to find the energy conservation from Eqs.(1) and (2) that

$$|\mathcal{E}(\hat{z})|^2 + \langle\eta\rangle = 0. \quad (3)$$

The other constant of motion comes from adiabatic invariant of action variable. If the change of fraction of undulator tapering is slow compared with the synchrotron oscillation period Ω_{syn}, the corresponding action variable can be still considered as a constant of motion and is expressed

$$\frac{\langle\eta - \eta_R\rangle^2}{2\Omega_{\text{syn}}(\hat{z})f_R(\hat{z})} + \frac{2f_B(\hat{z})}{\Omega_{\text{syn}}(\hat{z})f_R(\hat{z})}|\mathcal{E}(\hat{z})|\langle\sin(\theta + \phi)\rangle = 0. \quad (4)$$

Below in this subsection we take advantage of Gluckstern *et al.* [2] to parameterize the radiation field solution based on the equilibrium solution. The equilibrium solution here is referred to as the solution evaluated at the starting location of the undulator tapering or the first-saturation location. For the solution of the radiation field, we take the following form

$$\mathcal{E} = (P + iQ)e^{i\Phi}, \quad (5)$$

where $\Phi \approx \kappa_0 + \kappa_1(\hat{z} - \hat{z}_0) + \frac{\kappa_2}{2}(\hat{z} - \hat{z}_0)^2$. Let us introduce the variable β for the subsequent analysis, $\beta = \theta - \theta_R - \Phi$, which represents the displaced electron phase and $\langle\beta'\rangle \approx 0$ in the equilibrium [2]. The two constants of motion, Eqs. (3) and (4), can also be expressed in the following forms,

$$P^2 + Q^2 + f_R\left[\langle\beta'\rangle - \kappa_1\right] + \eta_R = 0, \quad (6)$$

and

$$\frac{f_R}{\Omega_{\text{syn}}}\left\{\frac{\langle\beta'^2\rangle}{2} - \kappa_1\langle\beta'\rangle + \frac{\kappa_1^2}{2} + 2\frac{f_B}{f_R^2}\left(P\langle\sin\beta\rangle + Q\langle\cos\beta\rangle\right)\right\} \approx 0. \quad (7)$$

It has been known that the equilibrium (or unperturbed) electron beam phase space distribution satisfies the Vlasov

02 Photon Sources and Electron Accelerators

A06 Free Electron Lasers

equation. The unperturbed solution can always be expressed in an arbitrary function of the constant(s) of motion. From the above analysis we have made the choice of using the action variable as an invariant. In what follows we adopt the Boltzmann-type distribution as the unperturbed solution [2]. It can be written in the form $f_{\mathrm{BZM}} = \mathcal{N} e^{-\alpha \tilde{I}(\beta, \beta'; \hat{z})}$, where $\mathcal{N}$ is the normalization coefficient such that $\langle f_{\mathrm{BZM}} \rangle \equiv \int_{0}^{2\pi} \int_{-\infty}^{\infty} d\beta d\beta' f_{\mathrm{BZM}}(\beta, \beta') = 1$, and α is a measure of the particle spread in the ponderomotive potential well [3]. From Eq. (7) we take $\tilde{I}(\beta, \beta'; \hat{z}) = \frac{f_R}{2\Omega_{\mathrm{syn}}}(\beta' - \kappa_1)^2 + \frac{2f_B}{\Omega_{\mathrm{syn}}f_R} P \sin\beta$. For convenience we also define $\chi = f_B/\Omega_{\mathrm{syn}}$, and $\mathcal{K} = \alpha f_R/\Omega_{\mathrm{syn}}$. Several relevant quantities can be evaluated, including the normalization coefficient $\mathcal{N} = \frac{\sqrt{\mathcal{K}}}{(2\pi)^{3/2} I_0(2\alpha\chi P)}$. Furthermore, the bunching parameters can also be evaluated $\langle \sin\beta \rangle = -\frac{I_1(2\alpha\chi P)}{I_0(2\alpha\chi P)} \approx -\alpha\chi P \equiv -\bar{s}$, where I_0 and I_1 are respectively the zeroth- and first-order modified Bessel function of the first kind, $\langle \cos\beta \rangle = \cos\Theta_R$, and $\langle \beta'^2 \rangle = \mathcal{K}^{-1} + \kappa_1^2$.

Now we will extend the 1-D wave equation to axisymmetric 2-D equation including the radial dependence of the radiation field. The analysis will include the diffraction effect and the guiding properties formed by the bunched electron beam through the FEL process. The electron beam now features a finite transverse size but the finite-emittance effect is still neglected. The radiation diffraction effect is included in the transverse Laplacian operator and the wave equation can be written as

$$\frac{\partial \mathcal{E}}{\partial \hat{z}} - i \nabla_\perp^2 \mathcal{E} = \frac{f_B(\hat{z})}{f_R(\hat{z})} U(\hat{r}) \langle e^{-i\theta} \rangle, \tag{8}$$

where $U(\hat{r})$ is the transverse electron beam profile and the scaled radius $\hat{r} = \sqrt{4\rho k_u k_R} r$. $\nabla_\perp^2 = \hat{r}^{-1} \partial/\partial\hat{r} (\hat{r}\partial/\partial\hat{r})$. In the absence of the right hand side (RHS) term, Eq. (8) becomes the paraxial Helmholtz equation and the solution can be typically parameterized by the Gaussian beam [4]. The presence of nonzero term on RHS of Eq. (8) acts as an external medium. This medium, due to electron beam microbunching, leads to an effective index of refraction greater than unity [5]. The two constants of motion now become

$$\int \hat{r}d\hat{r} P^2(\hat{r}; \hat{z}) = (f_R\kappa_1 - \eta_R) \int \hat{r}d\hat{r} U(\hat{r}), \tag{9}$$

and

$$\int \hat{r}d\hat{r} U(\hat{r}) \langle (\beta' - \kappa_1)^2 \rangle = \frac{2}{f_R} \int \hat{r}d\hat{r} \left[\kappa_1 P^2 + (\nabla_\perp P)^2 \right]. \tag{10}$$

Now we can solve the field equation, together with the constants of motion in a given transverse electron beam profile. Let us consider the simplest case, i.e., the uniform stepped profile $U(\hat{r}) = 1$ for $\hat{r} \leq \hat{R}$ and 0 for $\hat{r} > \hat{R}$. Here $\hat{R} = \sqrt{4\rho k_u k_R} R$ is the boundary of the transverse electron beam density profile. Substituting into Eq. (8) and expressing $\mathcal{E}$ in terms of P and Q, the resultant 2-D field equation can be analytically solved. Imposing the continuity condition at

the beam boundary $\hat{r} = \hat{R}$ gives a constraint and the explicit expression of the radiation field solution can be written as

$$P(\hat{r}; \hat{z}) = \begin{cases} \mathcal{A} J_0(\mu\hat{r}), & \hat{r} \leq \hat{R} \\ \mathcal{A} \frac{J_0(y)}{K_0(x)} K_0\left(\sqrt{\kappa_1}\hat{r}\right), & \hat{r} > \hat{R}, \end{cases} \tag{11}$$

where $x = \sqrt{\kappa_1}\hat{R}$, $y = \mu\hat{R}$, and $\mu = \sqrt{\alpha\chi f_B/f_R - \kappa_1}$. $\mathcal{A}$ is the on-axis field amplitude, J_0 and K_0 are the zeroth order ordinary Bessel function and the modified Bessel function of the second kind, respectively. Substituting Eq. (11) into Eqs. (9) and (10) we obtain

$$f_R\kappa_1 - \eta_R = \mathcal{A}^2 \left\{ J_0^2(y) + J_1^2(y) + \frac{J_0^2(y)}{K_0^2(x)} \left[K_1^2(x) - K_0^2(x) \right] \right\} \tag{12}$$

and

$$\kappa_1^2 = 2\alpha\chi \frac{f_B}{f_R} \mathcal{A}^2 \left[J_0^2(y) + J_1^2(y) \right] - \frac{1}{2\mathcal{K}} \tag{13}$$

Note that Eqs. (11-13) are to be solved for κ_1, α, and $\mathcal{A}$. Of our particular interest the combined term ($f_R\kappa_1 - \eta_R$) represents the FEL power efficiency, i.e., $f_R\kappa_1 - \eta_R = \frac{\int \hat{r}d\hat{r} P^2(\hat{r}; \hat{z})}{\int \hat{r}d\hat{r} U(\hat{r})}$. The electron energy spread will increase during the saturated FEL process and can be characterized by the scaled energy spread $\langle (\eta - \eta_R)^2 \rangle = \frac{\Omega_{\mathrm{syn}}}{\alpha}$, where the Jacobian due to the coordinate transformation, $\left| J\left(\frac{\partial(\theta, \eta)}{\partial(\beta, \beta')} \right) \right| = f_R$ is introduced.

NUMERICAL RESULTS

Let us illustrate how the saturated power efficiency and the effective width of the radiation field profile are affected by the undulator tapering. Figure 1(a) and (b) show the dependence of the power efficiency on the scaled transverse electron beam size and the taper ratio, respectively. Unlike the untapered case, the tapered power efficiency has very weak dependence on the transverse electron beam size. Going from $\hat{R} = 0.1$ to $\hat{R} = 5$ the theoretical predictions give 0.1% and 0.02% difference for transverse uniform distribution for the untapered and 1% taper case, respectively. The difference becomes even smaller for 8% taper ratio. The dots in Fig. 1(a) are obtained from the full 3-D numerical simulation GENESIS [6], where we can see both the theoretical predictions and the numerical results match well for the untapered and 1% taper cases. For 8% taper case, there appears a systematic deviation between the theoretical and simulation results. However the independence of the transverse electron beam size is shown. By looking at another dimension of the power efficiency dependence, the power extraction efficiency is now almost linearly dependent on the taper ratio, as shown in Fig. 1(b). It is interesting to note that when the taper ratio approaches to zero, i.e., the untapered case, the power efficiency reaches a constant close to the FEL or Pierce parameter ρ. It is further confirmed here that in the beam-wave matched case the resultant power efficiency can be close to, but still slightly smaller than, the total taper ratio. In view of Fig. 1, we remind that the above argument

02 Photon Sources and Electron Accelerators

A06 Free Electron Lasers

of power efficiency scaling does not apply to any arbitrarily large transverse beam size and to any level of taper ratio. The aforementioned discussion assumes negligible electron detrapping.
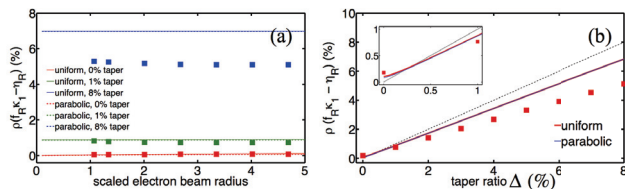

Figure 1: The dependence of the power efficiency on the scaled transverse electron beam radius (a) for three specific taper ratios (untapered, 1% and 8% taper ratios), and the dependence on the taper ratio (b) for the uniform transverse beam profile. The dots in (a,b) indicate the full 3-D numerical simulation results from GENESIS for the electron transverse uniform distribution. The inset in (b) shows the crossing of the calculated power efficiency to the $y = x$ dotted line.

Below we also illustrate the dynamics of the radiation field profile by using the full 3-D time-independent simulation code GENESIS. This numerical illustration enables us to see a clear picture how the spatial evolution of the radiation field intensity in both transverse and longitudinal dimensions, and the impact of undulator tapering. In the numerical simulation the electron beam transverse profile is set uniform round with the half width $\approx 28\ \mu m$ in x and y (or $\approx 40\ \mu m$ in r) and the total length of the undulator is assumed 70 m with $\lambda_u = 2.6$ cm. The corresponding radiation wavelength is 3.1 Å. The first saturation power ≈ 22 GW is matched at the beam waist with the input electron beam. The transverse domain in the numerical setup extends from -0.8 mm to $+0.8$ mm with a total number of 451×451 grid points to avoid possible numerical effects occurred along the boundaries. In the numerical simulation the undulator tapering starts at the very beginning with an overall taper ratio of continuous and quadratic 8%. Figure 2(a) shows the mountain-range plots for the evolution of the radiation intensity profile for both untapered and 8% tapered cases, where the clear broadening of the radiation field intensity in the 8% tapered case is indicated. More quantitatively Fig. 2(b) shows the evolution of the half-width half maximum of the radiation intensity profile. We see the transverse pulse broadening proceeds after $z > 20$ m. Besides, more and more of the enhanced radiation field intensity due to undulator tapering is contributed from outside of the transverse electron beam than from inside of it. By quantifying the ratio of the sum of field intensity inside the transverse electron beam size to that outside the beam, as shown in Fig. 2(c), we can see a decrease trend in the curve for the 8% tapered case after $z > 20$ m. The on-axis field intensity will therefore grow at a relatively slower rate than the transversely integrated field intensity.
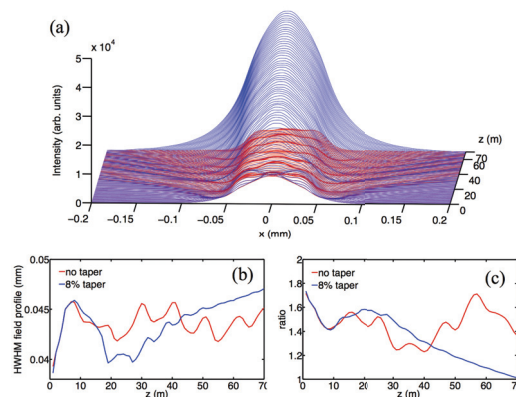

Figure 2: Three-dimensional mountain-range plot (a) for the evolution of the radiation field intensity for the untapered (red) and 8% tapered (blue) cases. The initial transverse electron beam profile is assumed uniform within $\approx \pm28\ \mu m$ in x and y (or $\approx \pm40\ \mu m$ in r). (b) The z-dependence of the half-width half maximum of the intensity profile. (c) The z-dependence of the ratio of the integrated field intensity outside the electron beam to that inside the beam.

SUMMARY

In this paper we have analyzed the post-saturation dynamics in a single-pass high-gain tapered FEL, including the power efficiency, the induced energy spread, and the radiation field intensity as a function of the scaled transverse electron beam size and the the level of undulator tapering. By taking advantage of two integrals of the motion, one from the energy conservation and the other from the action variable based on the adiabatic invariance of the undulator tapering, we have studied one case that allows analytical solutions of the radiation field: the uniform transverse electron beam profile. For another analytically solvable case, the bounded parabolic beam profile, we refer the interested reader to Ref. [7] for more details. The self-consistent solutions allow us to clearly see the dependences of the FEL power efficiency, the induced energy spread increase, and the broadening of the radiation field intensity on both the transverse electron beam size and the taper ratio.

It is found that the tapered power efficiency has weak dependence on the transverse electron beam size and can be greatly improved by virtue of undulator tapering up to its total taper ratio prior to occurrence of significant electron detrapping. In the presence of undulator tapering, besides the total power is enhanced (compared with the untapered case), it is also found that more and more the field intensity is contributed from outside of the transverse electron beam than from inside of it, consistent with the numerical observation in Ref. [8]. Finally we use a full three-dimensional time-independent simulation [6] to illustrate the spatial evolution of the radiation field intensity for an untapered and a 8% tapered case. The results are consistent with the conclusion made in our theoretical analysis for broadening of the radiation beam profile in the presence of undulator tapering.

REFERENCES

[1] R. Bonifacio *et al.*, "Collective instabilities and high-gain regime in a free electron laser", *Optics Communications*, vol. 50, p.373, 1984.

[2] R. Gluckstern *et al.*, "Analysis of the saturation of a high-gain free-electron laser", *Phys. Rev. E*, vol. 47, p.4412, 1993.

[3] Z. Huang and K.-J. Kim, "Transverse and temporal characteristics of a high-gain free-electron laser in the saturation regime", *NIMA*, vol. 483, p.504, 2002.

[4] B. E. A. Saleh. and M. C. Teich, *Fundamentals of Photonics*, Wiley Series in Pure and Applied Optics, 1991.

[5] E. T. Scharlemann *et al.*, "Optical Guiding in a Free-Electron Laser", *Phys. Rev. Lett.*, vol. 54, p. 1925, 1985.

[6] S. Reiche, "GENESIS 1.3: a fully 3D time-dependent FEL simulation code", *Nuclear Instruments and Methods in Physics Research Section A: Accelerators, Spectrometers, Detectors and Associated Equipment*, vol. 429, pp. 243-248, 1999.

[7] C.-Y. Tsai *et al.*, "Single-pass high-gain tapered free-electron laser with transverse diffraction in the post-saturation regime", *Phys. Rev. Accel. Beams*, submitted for publications, 2018.

[8] B. Hafizi *et al.*," Efficiency enhancement and optical guiding in a tapered high-power finite-pulse free-electron laser", *Phys. Rev. Lett.*, vol. 64, p. 180, 1990.